

# Micromirror-based sending and detection optical assembly for time-of-flight laser scanners

Britta Satzer<sup>a</sup>, Claudia Baulig<sup>a</sup>, Thilo Sandner<sup>b</sup> and Stefan Schwarzer<sup>a</sup>

<sup>a</sup>Fraunhofer-Institut für Physikalische Messtechnik IPM, Heidenhofstr. 8, 79110 Freiburg, Germany; <sup>b</sup>Fraunhofer-Institut für Photonische Mikrosysteme IPMS, Maria-Reiche-Str. 2, 01109 Dresden, Germany

## ABSTRACT

We design the optical unit for an imaging time-of-flight scanner camera based on partially steerable micro mirrors. This new class of 3D cameras enables video frame rates and—in conjunction with the accompanying user software—online real-time selection of regions of interest.

The challenges for the optical design comprise (i) sufficient light collection from close-up objects, (ii) maximizing optical efficiency for objects at large distances, (iii) reduction of the dynamical range of signal returns and (iv) minimization of parasitic scattering.

We present a solution based on coaxial beam guidance, where the emitted beam first passes a beam splitter, is then deflected by a dedicated emission mirror in the center of a point-symmetrical, synchronized arrangement of five micro mirrors and finally passes a protective spherical glass cover. The mirror assembly is slightly displaced from the center of the dome in order to establish a secondary focus for parasitic reflections at the inside of the cover. The light scattered at the target surface which reaches the mirror array is directed towards an assembly of rhomboid prisms. These prisms reshape the distributed mirror array aperture such that a small lens with high numerical aperture suffices to focus the light onto a fast, small-area avalanche photo diode, thus maximizing the acceptance angle of the detector and permissible misalignments of the element mirrors.

**Keywords:** micro mirror, MOEMS, micro mirror array, scanner, time-of-flight method, pulse measurement, optical design, dome

## 1. INTRODUCTION

Existing range image delivering camera systems are based on two fundamentally different approaches. First, a geometric principle is used as happens in photogrammetric or stereoscopic systems that derive range information from the comparison of two images of a scene taken from different positions or in systems using a combination of a projection and a capture device which obtain the range information from the distortion of the projected pattern. In this paper, we concentrate on a second class of devices uses time-of-flight information obtained by active illumination of the scene in combination with specific dedicated sensors to analyze the time that light needs for the roundtrip from the illumination over the object surface to the sensor (time-of-flight or TOF sensors). Some special requirements as, e. g. high accuracy or large measurement range in surveying, have often called for scanner systems that measure the distance to one or a small set of points and employ a mechanical scan device to sweep over the scene in order to generate a depth image.

Conventional time-of-flight (TOF) cameras employ a CMOS focal plane array chip<sup>1-3</sup> with a complex pixel structure. Illumination of the object surface enables the photo sensor and signal processing associated with each pixel to determine simultaneously the distance to all points of the scattering surface within the camera's field of view (FOV). While TOF cameras are compact and can be mass produced, the required modulated illumination of the entire FOV renders them sensitive to the lighting conditions and in particular to the shot noise component of the background light. In contrast to TOF cameras, laser scanners employ only a single detector element.<sup>4-7</sup> Scanners concentrate laser light on the smallest feasible spot (which determines the resolution of the scan) and the sensitive element typically collects light from a narrow FOV, ideally only marginally wider than the illumination

---

Corresponding author: Britta Satzer, [britta.satzer@ipm.fraunhofer.de](mailto:britta.satzer@ipm.fraunhofer.de), telephone: +49 761 8857-294

	TACO sensor	Swiss Ranger SR4000 <sup>2</sup>	ECO SCAN <sup>9</sup>
distance range (reflectivity)	0.15 - 7.5 m (0.1)	0.1 - 10 m	0.3 - 5 m (0.12)
depth resolution (repeatability)	3 - 5 mm	4 - 18 mm <sup>(i)</sup>	12 mm
angular resolution	$\leq 2$ mrad <sup>(ii)</sup>	4.2 mrad	
field of view	$90^\circ \times 50^\circ$	$69^\circ \times 56^\circ$	$60^\circ \times 50^\circ$
frame rate	$> 20$ Hz (240 $\times$ 160)	50 Hz	20 Hz
scan points per scan line	312 <sup>(iii)</sup>	176 ( $\times$ 144)	43 ( $\times$ 25)
3D point rate	1 MHz	1.27 MHz <sup>(iv)</sup>	$\approx 24$ kHz <sup>(iv)</sup>

Table 1. Target specifications of the TACO sensor in comparison with one scanner and focal plane TOF 3D cameras. <sup>(i)</sup> at reflectivity of 0.99; <sup>(ii)</sup> based on beam divergence; <sup>(iii)</sup> resolution can be increased by interlacing; intrinsic upper limit for scan lines, minimum  $\approx 20$ ; <sup>(iv)</sup> calculated from frame rate and frame resolution

spot. However, to sweep the image space, conventional scanners use heavy moving mechanical elements, which are subject to wear and increase size, sensitivity to vibration and environmental conditions as well as cost of the system. Here, we wish to combine the measurement principle of laser scanners with the advantages of steerable micro mirrors with two degrees of freedom in order to demonstrate the feasibility of a compact, potentially cheap design of an adaptive camera with a high accuracy in depth and lateral direction. The development takes place in the framework of the EU FP7 STREP project TACO.<sup>8</sup>

Existing systems<sup>9,10</sup> use two-axis fully resonant micro mirrors in order to realize Lissajous scan patterns to sweep the image space. Unfortunately, much scan time is thus spent in the turning points of the nearly harmonic motion close to the edges of the image frame while point density is lowest at the image center.

Though it is possible to construct steerable micro mirrors, e. g. for laser projection applications, commercially available versions have limited scope of applicability for a scanner camera. If mirror area is sufficiently large for light collection (see below, we will require 5 mm aperture), size comes at the cost of low resonance frequency which would imply frame rates well below video rates. E. g., Mirrorcle's<sup>11</sup> largest mirror capable of two dimensional vectorial control has 3.6 mm diameter, and permits  $\pm 10^\circ$  of mechanical tilt at about 400 Hz of resonant operation. At 20 Hz frame rate, frames will comprise only 40 lines, counting the two half periods separately, which is generally inadequate.

Our system will be built around a mirror with two degrees of freedom. It features one resonant and one steerable axis of size  $2.4 \times 3.6$  mm. The resonance frequency of the resonant axis is 1.6 kHz, that of the quasi-static axis is 120 Hz,<sup>8,12,13</sup> mechanical deflection  $\pm 22.5^\circ$  around the resonant and  $\pm 12.5^\circ - \pm 15^\circ$  around the quasi-static axis. In the TACO system, we aim at delivering  $160 \times 240$  pixel frames at rates of 20 to 25 Hz with a FOV of about  $90^\circ \times 50^\circ$ .

In this paper we will first introduce the overall system concept and target specifications of the TACO micro-mirror scanner camera and then address one by one the challenges that arise in the context of the implementation of the optical assembly for 2D micro mirrors and distance measurement with pulse TOF electronics.

## 2. SYSTEM CONCEPT

The system implementation concept emerges as a consequence of some of the design targets that result from our desire to build a 3D sensor which is superior to focal-plane TOF cameras with respect to the precision and reliability of the distance measurement at maintained frame rate. Our target specifications are summarized in table 1.

The first two specifications concern the TOF measurement method, whose precision and range performance is predominantly determined by: (i) the available signal light (constrained by eye safety), (ii) the efficient reception aperture (given by the effective area of the micro mirror elements) and (iii) the performance characteristics of the TOF measurement method itself.

In addition, the desired lateral resolution sets a lower limit on the acceptable mirror size since it determines the possible laser beam divergence by diffraction effects; we refer to the full cross-section angle as  $\beta$ . Given a Gaussian beam before being reflected off the mirror, we estimate that  $\beta = 1.5\lambda/a$  will determine our asymptotic resolution.

Here,  $a$  is the effective (projected) diameter of the mirror and  $\lambda$  the laser wavelength. From  $\lambda = 1550$  nm (see below) we obtain a minimum effective mirror diameter  $a \approx 1.1$  mm.

Key features of a 3D camera are its frame rate, resolution and scanned field of view. We use micro opto-electro-mechanical elements (MOEMS) designed for this project by Fraunhofer IPMS. As mentioned in the introduction, they enable video frame rates and scan angle of  $90^\circ \times 50^\circ$ .

The required high resonance frequencies in combination with the large mirror scan angle compete with the scanner requirement of the maximum possible effective mirror area for light collection. In order to reach the design goal for the measurement range, we chose pulse TOF measurement. The signal-to-noise ratio that is necessary for return pulse detection is determined by the measurement principle and implementation and defines the minimum amount of signal light required on the detector. The required optical area is thus proportional to the upper limit of the desired measurement range. Furthermore, the large scan angle requires oblique beam incidence (see below) on the mirrors which also increases the necessary mirror surface. Within the constraints mentioned in the last two paragraphs, an elliptical mirror geometry of  $2.6 \times 3.6$  mm has been implemented by Fraunhofer IPMS.

The available laser signal power is determined by eye-safety constraints.<sup>14</sup> It is advantageous to work in a regime, where the laser radiation is not focused onto the retina of the eye, but absorbed in the aqueous cornea as is the case for wavelengths longer than 1500 nm. Summarized in a simplified fashion, in this case the eye safety of a pulse measurement system is given if on average less than about 10 mW of laser signal power can fall onto the eye. As it is comparatively simple to maintain and monitor the correct state of motion of the resonant axis, we decided to not rely on the additional motion in quasi-static direction. The largest density of measurement points occurs at the turning points of the motion. Consequently, by obscuring this part of the mirror trajectory to the outside, the possible irradiation of the eye is greatly reduced. We arrive at  $\approx 500$  W permissible laser peak power (pulse length 1 ns, repetition rate 1 MHz) by sacrificing about 20% of the scan range of the resonant axis.

A critical signal-to-noise level—where the standard deviation of repeated measurement will exceed 5 mm—is reached at 1  $\mu$ W signal power. Thus, the object distance where our optical system collects a fraction of  $2 \times 10^{-8}$  of the emitted laser light defines the threshold distance for reliable measurement of a Lambertian surface of 10% reflectivity. We will consider this distance as the upper limit of the measurement range.

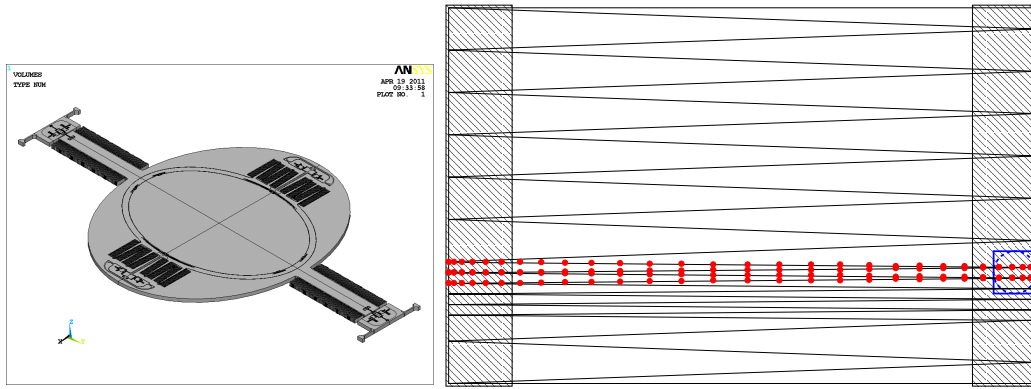
It turns out that the measurement range set out in Table 1 cannot be achieved with the aperture that a single mirror element provides and we must thus combine multiple mirrors into one array. The necessary synchronization effort for the array increases with the number of mirrors. This effort in conjunction with size constraints for the array geometry—depending on the filling factor of the MOEMS structures—sets the number of mirrors to five (or six). The entire aperture of the array is then equivalent to a circle of about 5 mm diameter.

### 3. OPTICAL DESIGN

As the final mirror configuration, we picked an arrangement of five identical micro mirrors. A central mirror, used both for beam emission and reception, is surrounded in point symmetrical fashion by four additional peripheral mirrors. Details on the considerations entering the array construction will be reported elsewhere.

Fig. (3) demonstrates how the mirror array is integrated into the overall optical design. Let us first discuss the setup from the perspective of the scanned laser beam. The collimated Gaussian beam generated by a fiber amplifier first passes a 50:50 beamsplitter and hits the central mirror at an angle of about  $30^\circ$  to the mirror normal at rest in vertical scan direction. As can be seen in Fig. 3, which shows the detailed geometry as employed in the optical simulations, the necessary minimum incidence angle depends on the size of the mirror array and its distance from the reception optics. Here for a given array size, the angle can only be decreased at the expense of a larger dome diameter; we will see below that the position of the array within the optical assembly cannot be changed at will.<sup>15</sup>

To avoid undesired reflections, the micro-mirror array has no protective cover. Thus, after reflection from the mirror surface, the laser beam hits the exit window, a glass dome, from a slightly off-center position. The reflexes from the interior and exterior surfaces of the dome are directed independent of both directions of scanning angles to a conjugate spot, positioned symmetrically with respect to the dome center in its “empty” half, cf. Fig.3,



a)

b)

Figure 1. The gimbaled micro mirrors are characterized by one resonant scan axis with 1.6 kHz resonance frequency (horizontal, optical scan angle  $90^\circ$ ) and a second quasi-static axis capable of motion with up to 120 Hz (vertical, resonant optical scan angle  $60^\circ$ ). At the intended operating frequency (10 Hz, corresponding to 20 Hz frame rate), an optical angle of  $50^\circ$  is possible and motion can be controlled in a mostly vectorial manner. In the scanner camera we use vectorial control to implement scanning with variable scan line densities, indicated in the lower half of the figure. At constant measurement rate, average intensity of the laser is highest at the turning point of the motion. For the TACO sensor, we obscure these regions mechanically (hatched rectangles) to remain eye-safe while utilizing sufficient laser power to reach design specifications.

and of roughly 8 mm from the mirror surface, the laser beam hits the exit window, a glass dome, from a slightly off-center position. The reflexes from the interior and exterior surfaces of the dome are directed to a conjugate spot, positioned symmetrically with respect to the dome center in its “empty” half, cf. Fig.3, and of roughly 8 mm diameter. At that conjugate point we position a beam dump, because we need to avoid these reflexes reaching the detector—otherwise possibly producing returns indistinguishable from those due to real objects close to the sensor. If the mirror was located in the center of the dome, the reflex would travel along the inverted beam path and hit the detector of the TOF electronics with the consequence of causing a “dead time” which would render reliable measurements of surfaces very close (20 - 30 cm distance) to the dome impossible. In order to deal with weaker scattering signals due to pollution of or dust on the exit window we introduce a time gating for return signal processing in the framework of the TOF electronics.

With the present setup, only laser light scattered by objects exterior to the glass dome will return over the central mirror. It then passes the beamsplitter, where half of the return signal is directed towards the laser and the other half reaches the sensitive detector area via a prism and an aspherical focusing lens. Of course, the beamsplitter introduces a significant loss of signal power, both for the emitted beam of which half the power is lost in a beam dump and for the light received over the central mirror of which only 50% can reach the detector. However, the loss of signal power is only relevant for light reaching the detector over the central mirror, which we employ to detect close up objects that will produce strong returns. For the loss of beam power we compensate by additional amplification. Future improvements will consider the use of a polarized signal source in combination with a polarizing beamsplitter or non-symmetric beam splitting ratios.

The principal role of the peripheral mirrors is to contribute to the signal from objects “far” from the sensor. From Fig. 4 we see that the crossover from “near” to “far” range occurs between less than 1 m and about 2 m distance. Light from object surfaces in that range reaches the peripheral mirrors at angles small with respect to the optical axis (cf. Fig. 3). Please note, that the received light passes through different spots on the glass dome at non-perpendicular angles and thus each path is characterized by a specific small offset and aberration angle. The optical design ensures that despite these imperfections, light from objects farther than 2 m will be focused onto the detector.

The detector is a 200  $\mu\text{m}$  avalanche photo diode (APD), coupled to a fiber with the same core diameter. This component proved to be of sufficiently large bandwidth to meet TOF detector requirements while at the same

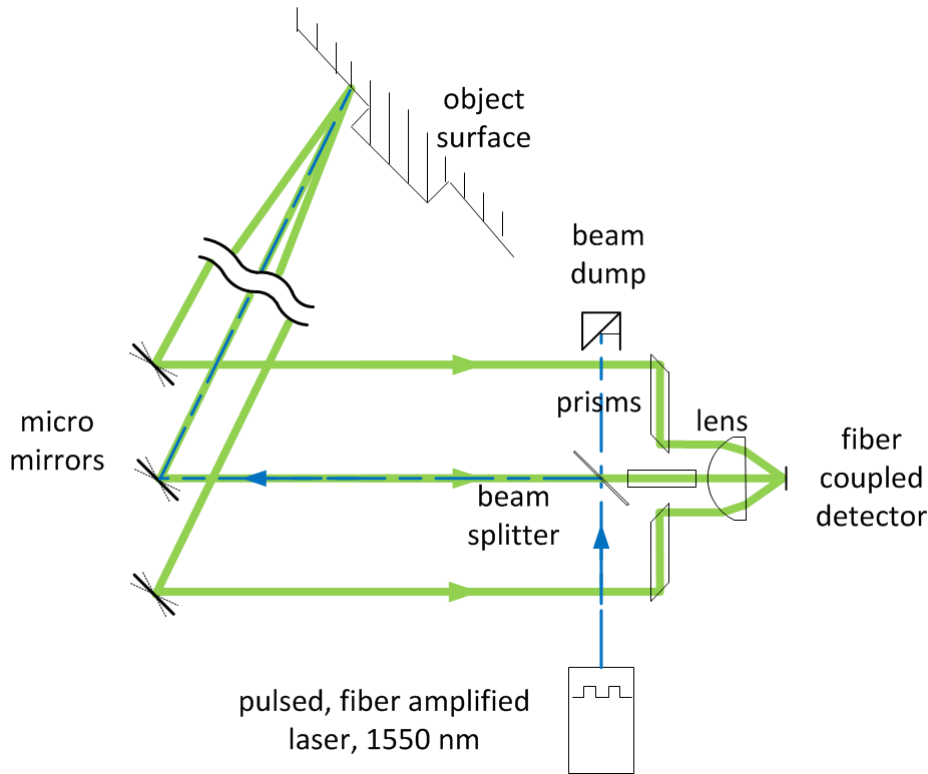


Figure 2. The figure illustrates the general optical concept. The laser beam is directed in oblique direction onto the center mirror via a 50:50 symmetric beamsplitter which also permits to use half of the signal light returned via that mirror, important for the detection of close-up objects. The source power is tuned to the maximum level compatible with eye-safety of the scanned beam outside the glass dome of the optical assembly. Typical object surfaces scatter into a wide solid angle; thus signal light is collected *a priori* by all mirrors. Rhomboid prisms direct the received light, if sufficiently parallel to the optical axis (defined by the straight line through the center of the emission mirror, beamsplitter and detector), onto a collecting lens without changing the incidence angle. The parallel shift enables us to use a significantly smaller aspheric lens with a short focal length. Furthermore, the rhomboid prisms serve as a kind of spatial filters for stray light not parallel to the optical axis or not originating from one of the mirrors.

to the lens. Furthermore, the rhomboid prisms serve as spatial filters for stray light not parallel to the optical axis or not originating from one of the mirrors.

time being sufficiently large to permit the detector FOV to accommodate the dome lensing effects noted above. Hence we chose the arrangement of four mirrors placed symmetrically around the sending mirror to achieve a close packing within the MEMS package dimensions and thus keep optical aberrations best possible small. Please note that the detector FOV  $\phi_d$  is determined by the focal length  $f$  of the light collecting asphere and the diameter  $a$  of the fiber core,  $\phi_d = 2\arctan(a/2f)$ . Maximizing detector FOV thus requires the largest possible detector area  $a$  and the smallest possible focal length  $f$ . Small focal length also necessitates a geometrically small lens as the f-number of lenses cannot be much smaller than 1. The geometrical size of the lens, however, is determined by the area needed to collect light parallel to the optical axis from all contributing mirrors. The small filling factor of the element mirrors suggest a solution involving light guides, here N-BK7 rhomboid prisms, to transfer light far from the optical axis closer to the optical axis (see Fig. 3).<sup>15</sup> Care needs to be taken to ensure the same optical path length for all possible ways onto the detector which we have addressed using a compensation prism of high-index N-SF66 glass for the center mirror. In this way, we have reduced the necessary lens diameter to about 12 mm and its focal length to about 10 mm. For this combination, we obtain  $\phi_d \approx 1.2^\circ$ . In Fig. 5 the resulting mapping of light from a selected mirror onto the opening of the fiber is shown for nine mirror deflections corresponding to the edges and the center of the sensor FOV. It can be seen that the focal spot position corresponding to one mirror moves over a large fraction of the fiber opening with changing pointing

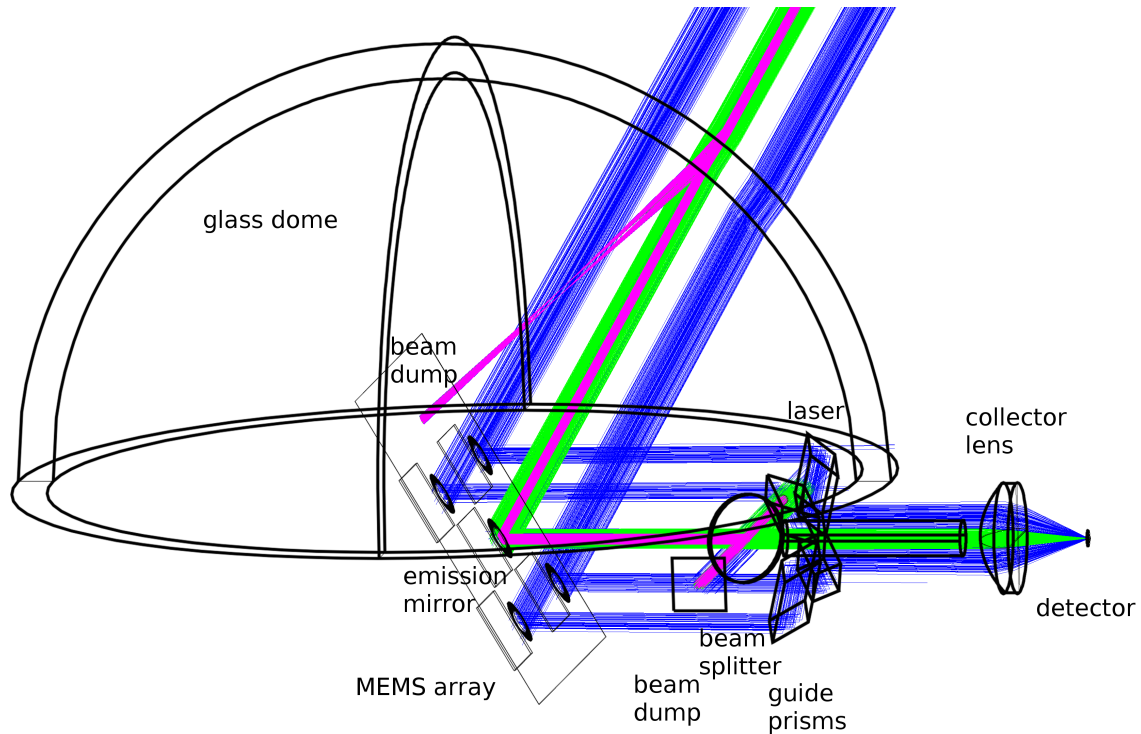


Figure 3. The detailed setup for the optical simulation and ray paths for the emitted beam in rest position of the micro mirrors and the received light corresponding to the sketch in Fig. 3. We see that a fraction of the emitted beam is reflected at the interfaces of the glass dome cover. To additional reflexes, the micro mirror array is not housed separately, but mounted and enclosed in a dust-free environment. The array is placed slightly off-center with respect to the dome, such that parasitic reflections are directed above the array and into a small region behind the MOEMS array. On base level of the array, the light falls through a small hole in an electronics PCB which extends to the limits of the dome and is caught mostly in the half-space behind that PCB. The rhomboid prism assembly must correct for the longer paths of signal light through the edge prisms and thus uses a high refractive index glass cylinder of appropriate length for light entering along the optical axis. The mostly parallel signal light emanating from the prisms falls onto a small lens with high numerical aperture that focuses the spots onto the  $200\ \mu\text{m}$  core of a fiber attached to the detector.

direction of the mirror.

The remaining distance from the rim of the fiber core sets the maximum permissible mirror misalignment to be around  $0.05^\circ$  (determined by simulation) which puts high demands on the circuitry used to drive the mirrors in a synchronized fashion and on the mechanical alignment of the mirrors with respect to the surrounding optical components.

The prism arrangement is optimized to capture light scattered off far surfaces, beam paths parallel to the optical axis have been assumed. In Fig. 4, we show as a function of the distance  $r$  of an object with an ideal Lambertian surface the simulated fraction of signal light with respect to the laser beam power at the entry of the optical assembly before the beamsplitter. At small distances we see the asymptotic  $1/r^2$  behavior due to light passing over the central mirror alone. At distances larger than about 2 m, the asymptotic behavior due to light captured by all five mirrors is seen. The two dashed lines in the figure denote the value that would result from ideal optical components (ideal reflection on the mirror, no absorption in glass) in the “near” and “far” asymptotic regions. The gap between the lines corresponds to a factor of 9 which results from the ratio of the entire available mirror surface to the emission mirror alone, where the emission mirror surface is counted only with a weight of  $1/2$  to account for the signal light loss in the symmetric beamsplitter.

Between about 1 and 2 m distance, a crossover occurs as the light entering via the peripheral mirrors becomes sufficiently parallel to the optical axis to be mapped onto the detector. In this region the prefactor of the inverse

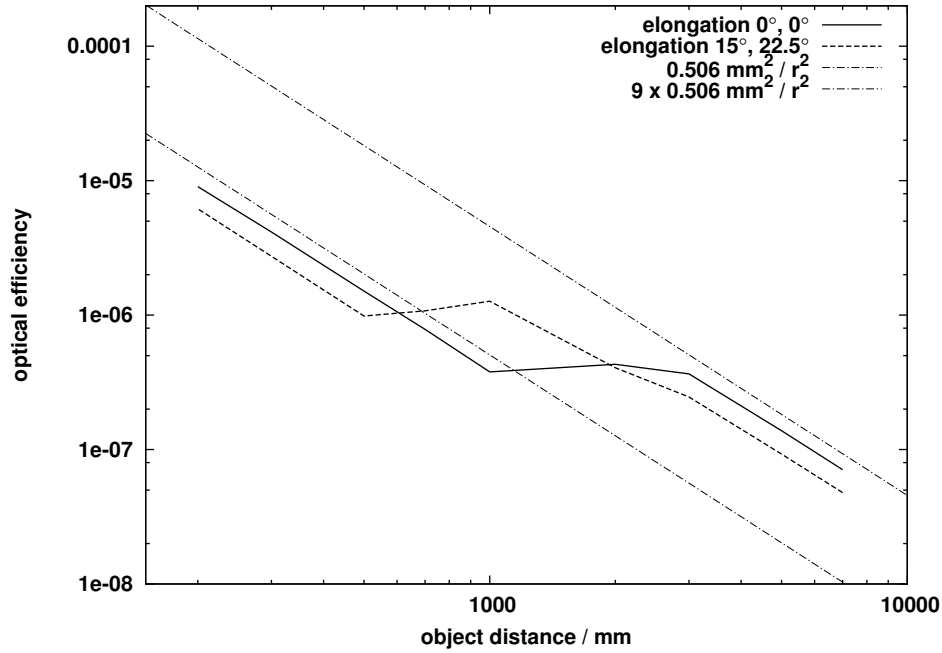


Figure 4. As results of optical simulations this graph shows the ratio between received signal and peak intensity of the sending beam as a function of the object distance while measuring on a white Lambertian scatterer. The two thick-line curves represent simulations for two representative positions of the micro mirrors, the mirror inclination is indicated in the legend inset. As guides to the eye, the dash-dotted lines correspond to theoretical curves assuming ideal optical components (lower line: contribution from the emission mirror alone, upper line: contributions of all five mirrors). Due to the double logarithmic scale, pure  $1/r^2$  behavior appears as a straight line which we also see for the simulated curves for very small and large distances. For large distances, where all mirrors contribute, the aperture is nine times higher than close up, where only the center mirror contributes. The asymptotical offsets between the simulated and the simplified theoretical curves are due to reflections at interfaces and absorptions in glass components.

square distance behavior changes by the geometric factor of 9 explained above. The overall effect of reducing the dynamic range below that of a pure  $1/r^2$  law is very desirable for the TOF electronics which depends on linear circuitry.

It should be noted here that the prisms serve an additional important purpose: their opening is chosen to match the mirror diameter. Light that passes through the opening either originates from the mirror and is parallel to the optical axis or if not originating from the mirror is also not parallel to the optical axis. The latter light will not (or only partially) be mapped onto the detector. The spatial filtering property is especially important to suppress signal light components resulting from stray light paths in the system. These will arise for example because the Gaussian beam tails will be partially scattered or reflected off the silicon substrate surrounding the mirrors; this substrate is structured and comprises the drive structures and the necessary conductive paths. The resulting signals from parasitic reflexes within the optical assembly itself will be suppressed by electronic means. If, however, the stray light is sufficient powerful to return on an inverted path due to scattering on the outside of the system and proceeds to the detector, it can only be distinguished from the desired reflex on the surface of a (sufficiently dark) object in the main beam path by image analysis and plausibility considerations at later stages in the system software. Additional supporting measures against the described risk include (i) choice of the smallest possible diameter of the collimated laser beam to reduce the fraction of light hitting the peripheral structures, (ii) electronic measures to separate closely spaced return pulses as well as possible to enable post-detection signal quality control.

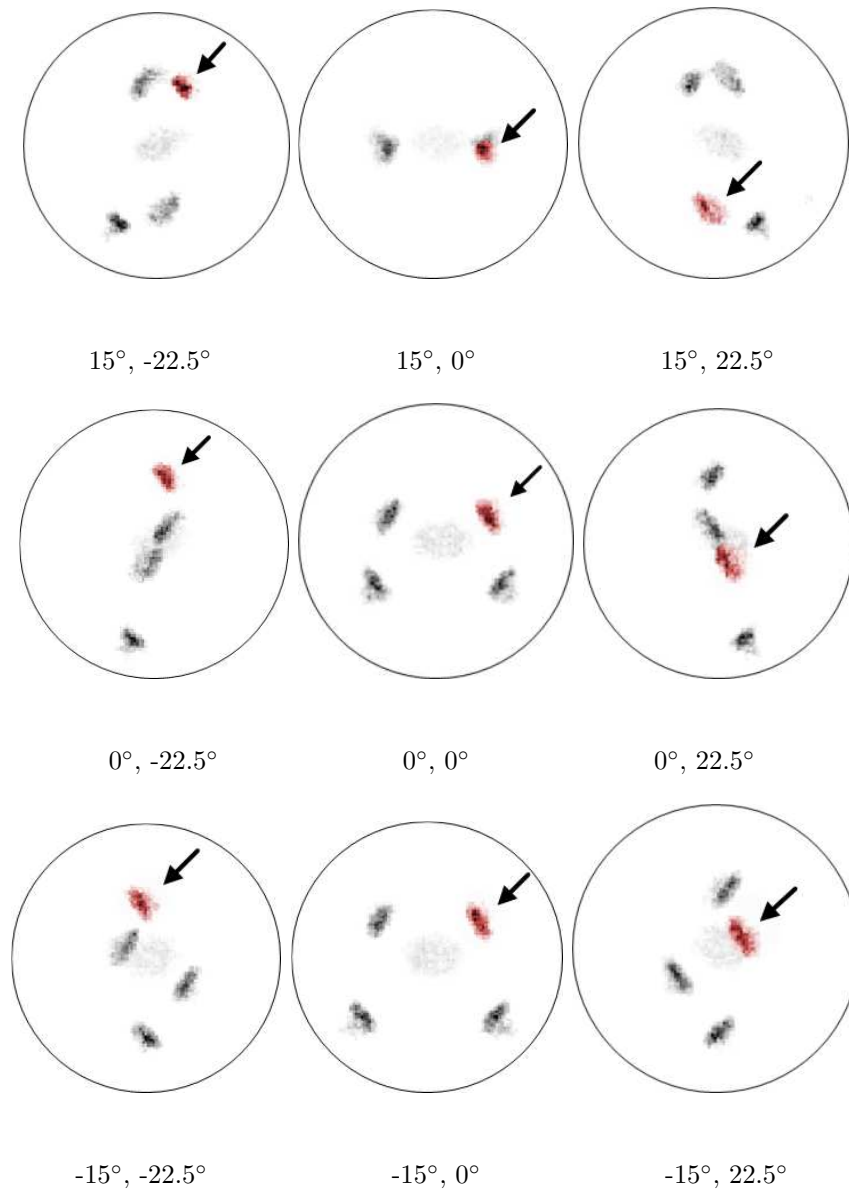


Figure 5. This figure shows the distribution of the “focal” spots corresponding to the different mirrors in the detector plane for an object in 7 m distance. Increasing darker grey corresponds to increasing irradiation on the detector. The pointing directions of the mirror array are indicated below each image and referred to the mirror normal at rest. The contribution of the mirror in the upper-right corner of the array as seen from the beam splitter is marked in each case and illustrates the wandering of the spots due to the optical aberration of the dome while scanning.

### 3.1 Conclusion

We have presented optical design considerations for a scanner camera based on an array of micro-mirrors with two degrees of freedom. We have shown solutions to address possible back reflexes from the glass housing of the optical unit by directing these reflexes into a secondary focal spot. Close-up surface detection is effected using a shared emission and reception mirror enabled by a beam splitter to join the outgoing laser beam and the incoming signal light paths. Prisms guide the reception light closer to the optical axis to optimize detector FOV in order to be tolerant to slight misalignments within the the mirror system. The crossover between reaction to close-up objects and objects at large distance has been employed advantageously for reduction of the dynamical

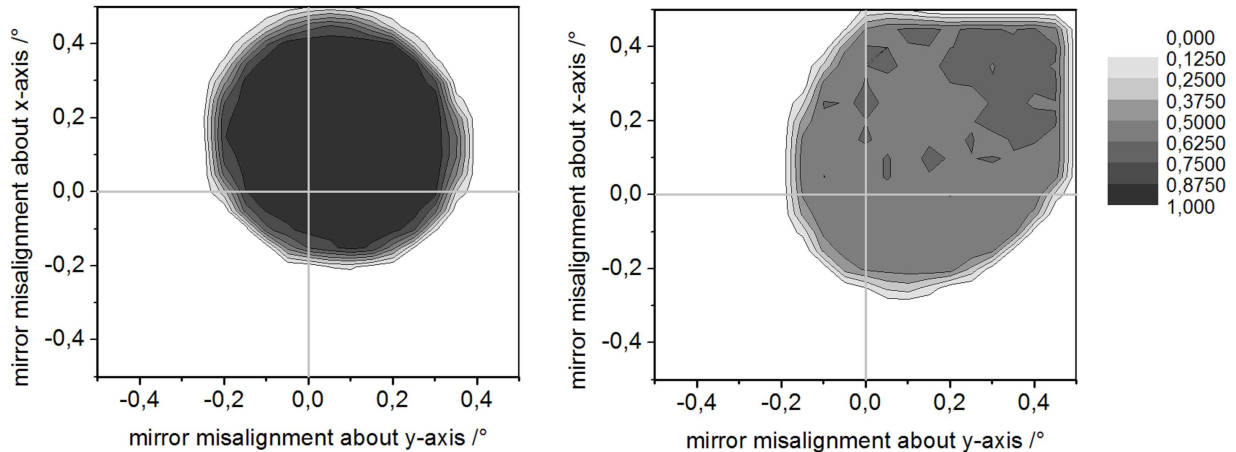


Figure 6. The diagrams shown visualize the influence of the mirror misalignment onto the reception intensity. The normalized intensity of the received rays of a single representative mirror (upper-right in the array as seen from the beam splitter) is plotted against the misalignment of reception and sending mirror. The left figure deals with the center scanning position while the right diagram results from a scan into the upper-left corner of the scan range. Since the mirror was tilted maximal for the right figure, the smaller aperture leads to a smaller maximum intensity there. Generally, the tolerances depend on the direction of the angular error. Though, as shown in figure 5, the spots move across the detection plane while scanning. Thus, only a small permissible misalignment of about  $0.05^\circ$  remains.

range that needs to be addressed in the TOF electronics. In conjunction with the time-of-flight unit, this optical system enables measurement from 0.15 m up to about 7 m.

### 3.2 Acknowledgments

We thank Ilia Bourovoi, Harald Wölfelschneider and other Fraunhofer IPM staff for many fruitful discussions about micro mirrors and optical concepts as well as the TACO EC FP7 consortium for many insights into the need of robotics and security applications. The research leading to these results has received funding from the European Union's Seventh Framework Programme (FP7/2007-2013) under grant agreement No. 248623.

### REFERENCES

- [1] PMD Technologies GmbH, data sheets, datenblatt\_camcube3.pdf, PMDvision-CamBoard-nano.pdf, www.pmdtec.com, access date:16.03.2012.
- [2] MESA IMAGING, data sheet, SR4000\_Data\_Sheet-1.pdf, 26.08.2011, <http://www.mesa-imaging.ch>, access date: 1.03.2012.
- [3] ifm electronic gmbh, data sheet, <http://www.ifm.com/products/de/ds/O3D201.htm>, access date: 16.03.2012.
- [4] Leica Geosystems AG, data sheets, leica\_scanstation\_c10\_ds.en.pdf, HDS7000\_DAT.en.pdf, <http://hds.leica-geosystems.com>, access date: 16.03.2012.
- [5] Zoller+Fröhlich, data sheet, Broschuere\_5010\_E.pdf, <http://www.zf-laser.com>, access date: 16.03.2012.
- [6] RIEGL Laser Measurement Systems GmbH, data sheet, Datasheet RIEGL VQ-450, 12.09.2011, www.riegl.com, access date: 16.03.2012.
- [7] H. Wölfelschneider, A Blug, C Baulig, and H Höfler. "Schnelle Entfernungsmessung für Laserscanner". *Technisches Messen*, 72:455–467, 2005.
- [8] TACO, Seventh Framework Programm, Programm acronym: FP7-ICT-2009-4, Start date: 2010-02-01, www.taco-project.eu, access date: 16.03.2012.

- [9] NIPPON SIGNAL CO.ECO SCAN, data sheet, FX8.pdf, <http://www.signal.co.jp>, access date: 15.03.2012.
- [10] C. Zhang, Z. You, H. Huang, and G. Li. "Study on a Two-Dimensional Scanning Micro-Mirror and its Application in a MOEMS Target Detector". *Sensors*, 10:6848–6860, 2010.
- [11] Mirrorcle Technologies, data sheet, Inc., Description.pdf, 2009, [www.mirrorcletech.com](http://www.mirrorcletech.com), access date: 16.03.2012.
- [12] T. Sandner, D. Jung, D. Kallweit, T. Grasshoff, and H. Schenk. "Microscanner with Vertical out of Plane Combdrive". *Int. Conf. on Optical MEMS Nanophotonics*, pages pp. 33–34.
- [13] D. Jung, T. Sandner, D. Kallweit, T. Grasshoff, and H. Schenk. "Vertical comb drive micro scanners for beam steering, linear scanning and laser projection applications". *MOEMS and Miniaturized Systems XI, Proc. SPIE 8252*, pages pp. 82520U–1–10.
- [14] Deutsche Norm: Safety of laser products-Part 1: Equipment classification and requirements (IEC 60825-1:2007). *German Version EN 60825-1:2007*, 2008.
- [15] C. Baulig and B. Satzer. "Sende- und Empfangsordnung". *Fraunhofer Institute for Physical Measurement Technics IPM, DE patent application, 10 2011 113 147.0*, 2011.